Available online at www.sciencedirect.com

ScienceDirect

Procedia CIRP 143 (2026) 45–48

www.elsevier.com/locate/procedia

14th CIRP Conference on Photonic Technologies

Comparison between laser welding modelling approaches: from low fidelity numerical simulation to high fidelity and Physics informed neural networks

Samuele Piandoro[a,*], Dexiang Zha[a], Erica Liverani[a], Alessandro Ascari[a], Alessandro Fortunato[a]

[a] *University of Bologna, Viale Risorgimento 2, Bologna, 40136, Italy*

* Corresponding author. *E-mail address:* samuele.piandoro2@unibo.it

Abstract

This paper presents a systematic comparison of three modelling frameworks for predicting weld bead geometry in laser beam welding: a low-fidelity (LF) thermal finite element model, a high-fidelity (HF) coupled thermo-fluid model, and a physics-informed neural network (PINN). The approaches are implemented, calibrated, and validated against experimental cross-sections from overlap welding of 6082-T6 aluminum alloy sheets. The influence of model architecture, physical assumptions, and mesh resolution on predictive accuracy and computational cost is discussed. Results show that while the HF model captures complex phenomena such as keyhole dynamics and surface deformation, both the LF model and the PINN achieve comparable accuracy in predicting weld bead dimensions at significantly lower computational cost. For PINNs specifically, a non-monotonic dependence of training performance on network architecture is identified, with an instability threshold linked to the total number of trainable parameters. These findings provide practical guidelines for model selection in laser welding process optimization.

© 2026 The Authors. Published by Elsevier B.V.
This is an open access article under the CC BY-NC-ND license (https://creativecommons.org/licenses/by-nc-nd/4.0)
Peer-review under responsibility of the scientific committee of the 14th CIRP Conference on Photonic Technologies [LANE 2026]

Keywords: Laser welding; Process modelling; physics-informed machine learning

1. Introduction

Laser beam welding (LBW) is a well-established technology for joining both similar and dissimilar materials [1], widely adopted in demanding industrial applications such as the automotive sector thanks to its high processing speed and non-contact nature. The demand for fast process optimization and real-time control has driven researchers towards new modelling approaches, as the traditional trial-and-error strategy is no longer sustainable in terms of time, cost, and resource consumption [2]. Numerical approaches are characterized by their level of fidelity [3]. Low-fidelity (LF) models rely on simplified heat sources and physical assumptions to provide rapid predictions, while high-fidelity (HF) models incorporate complex phenomena such as fluid dynamics and moving interfaces, achieving superior realism at the expense of high computational costs [4–6]. In parallel with traditional numerical modelling, machine learning techniques have increasingly been applied to laser-based manufacturing processes [7,8]. Neural networks map inputs into outputs through a layered architecture of artificial neurons, yielding a black-box surrogate with high predictive accuracy but limited physical interpretability and a strict requirement for large, labelled datasets, which are often difficult to obtain in welding applications. To address this limitation, physics-informed neural networks (PINNs) have emerged as promising alternatives. In those models the problem's physics, i.e. the partial differential equations (PDE) along with initial (IC) and boundary conditions (BC), are used to obtain a surrogate mapping between inputs and outputs. The model is optimized with limited or even without labelled data. A graphical comparison between the modelling approaches is shown in Fig. 1.

2212-8271 © 2026 The Authors. Published by Elsevier B.V.
This is an open access article under the CC BY-NC-ND license (https://creativecommons.org/licenses/by-nc-nd/4.0)
Peer-review under responsibility of the scientific committee of the 14th CIRP Conference on Photonic Technologies [LANE 2026]
10.1016/j.procir.2026.07.011

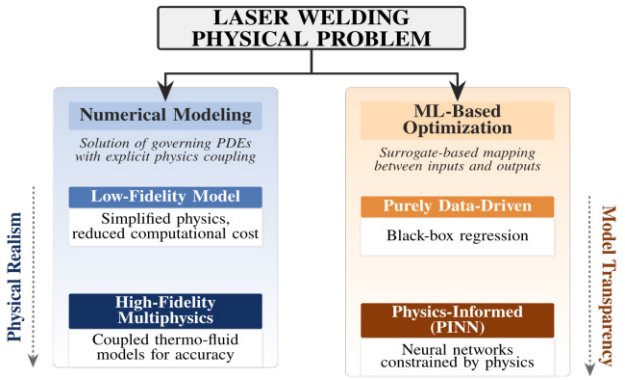

Fig. 1: Laser welding modelling approaches

This work presents a comparison of three modelling approaches for the prediction of an overlapping laser weld bead: a thermal low-fidelity numerical model, a coupled high-fidelity numerical model, and a physics-informed machine learning model. The implementation of each approach is described, highlighting key characteristics and strategies, and the most significant results, in terms of influence of model architecture, prediction capabilities, and computational cost, are discussed.

Materials & Methods

The study focused on overlapping welding of two 1.5 mm thick 6082-T6 aluminum alloy sheets. The welding setup comprised a Yb:fiber CW multi-mode source (nLight Alta, 2.5 kW) and an F-Theta galvo scanner head (Scanlab HurryScan 30), with a focal spot diameter of 65 µm (measured via PRIMES FocusMonitor). Six parameter combinations were tested: power level of 750, 1000, and 1500 W combined with speed of 0.1 and 0.3 m/s. Five conditions were used for model calibration, while the 1500 W – 0.3 m/s condition served as validation. Three cross-sections for each configuration were obtained by EDM and etched with Keller's reagent to reveal the weld bead geometry; The average weld bead depth and width were used as reference. A more detailed description of the models and procedure can be found in previous publications [6,8]

1.1. Numerical modelling

Two modelling approaches with different levels of fidelity were developed and tested. The FEM software COMSOL Multiphysics® (v6.3) was used to implement a low-fidelity thermal model, while a high-fidelity coupled thermal-fluid model was implemented in FLOW-3D Weld (v2025R1). The main features of each approach are summarized in Table 1. Both models are time-dependent and three-dimensional. A 3 mm weld length is simulated along the welding direction (x-axis), with the transverse (y) and through-thickness (z) dimensions selected to ensure adequate thermal dissipation. To reduce computational cost, the HF model exploits the geometric symmetry of the weld and simulates only half the domain in the y-direction, while the LF model uses the full domain.

Table 1 Comparison numerical modelling strategies

Feature	Low-Fidelity	High-Fidelity
Physics	Pure heat conduction	Coupled thermo-fluid dynamics
Numerical method	Finite Element	Finite volume
Mesh type	Tetrahedral	Structured cartesian
Laser modelling	Volumetric heat source	Ray tracing with multiple reflections
Phase change	Apparent heat capacity	Enthalpy
Fluid dynamics	None	Incompressible Navier-Stokes (laminar)
Surface tracking	None	Volume of Fluid
Density	Constant	Temperature dependent

Since no explicit phase change is modelled in the LF approach, an apparent heat capacity strategy was adopted, in which the temperature-dependent heat capacity is defined as follows:

$$C_p(T) = C_{p,sol} + \sum_i \frac{L_i}{\sqrt{\pi \Delta T^2}} \exp\left(\frac{(T-T_i)^2}{\Delta T^2}\right) \quad (1)$$

where the solid-phase heat capacity is augmented by contributions from the latent heat of melting and evaporation (index i). Material properties were taken from [9].

In contrast, the HF model explicitly accounts for both melting and vaporization and employs the Volume of Fluid (VOF) method to track the dynamic evolution of the interface between the keyhole and the surrounding gas.

The two models also differ in their laser source discretization. In the HF model, a discrete set of rays is generated and traced during their interaction with the material, enabling a physically realistic description of laser–material coupling, including multiple reflections inside the keyhole. In the LF model, the laser is treated as a volumetric heat source acting within the base material. Specifically, the double-cone volumetric source proposed by Farland [10] was adopted, defined by five geometric parameters: upper and lower heights H_u and H_l, and top, interface and bottom radii r_t, r_i and r_b. The heat input is given by:

$$Q_v = \frac{9\eta Q_j e^3}{\pi(e^3-1)V_j} \exp\left(-3\left(\frac{(x-vt)^2+y^2}{r_j^2}\right)\right) \quad (2)$$

$$\begin{cases} V_u = H_u(r_t^2 + r_t r_i + r_i^2), & r_u = r_t - (r_t - r_i)\frac{z}{H_u} \\ V_l = H_l(r_i^2 + r_i r_b + r_b^2), & r_l = r_i - (r_i - r_b)\frac{z_i - z}{H_l} \end{cases} \quad (3)$$

where subscript j refers to the upper (u) or lower (l) cone. The laser translates linearly along the x-direction at velocity v, with power distributed between the two cones in a ratio of 0.7:0.3. For both models, a uniform room-temperature initial condition was applied. The bottom surface was assigned to a fixed temperature, while the top surface was modelled as a pressure outlet (HF) or as a wall with convective and radiative heat loss (LF); all lateral surfaces were treated as adiabatic.

1.2. Physics-informed machine learning

A physics-informed neural network was developed in the PyTorch environment as an alternative to the LF thermal model, sharing the same governing equations, boundary and initial conditions. A schematic overview of the model architecture and training workflow is shown in Fig. .

Unlike both traditional numerical methods and conventional machine learning, PINNs enforce physical constraints without requiring spatial discretization or labelled training data. This is

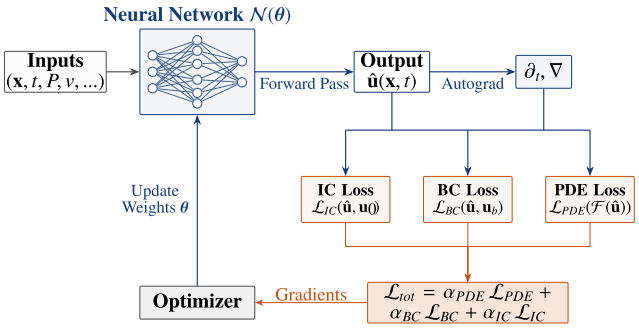

Fig. 2 PINN workflow

achieved by minimizing the residuals of the governing PDEs, BCs, and ICs at a set of collocation points sampled within the spatiotemporal domain, exploiting automatic differentiation (Autograd) to compute the necessary derivatives. The total loss function is therefore defined as a weighted sum of the PDE, boundary, and initial condition terms, as follows:

$$L_{tot} = \alpha_{PDE}L_{PDE} + \alpha_{BC}L_{BC} + \alpha_{IC}L_{IC} \quad (4)$$

The three weights were defined after a parametric study to ensure both fast and steady convergence, equal to 5000 for both the BC and IC components and 100 for the PDE residual. The total loss is minimized using the L-BFGS optimizer. The PINN is trained without any experimental data, that is only used after the convergence to calibrate the volumetric heat source geometric parameters against the laser power and speed.

2. Results and Discussions

The validation set of parameters (1500 W – 0.3 m/s) is used to assess the prediction capability with respect to model configuration. Fig. 3 shows the mesh independence study performed for the high-fidelity simulation.

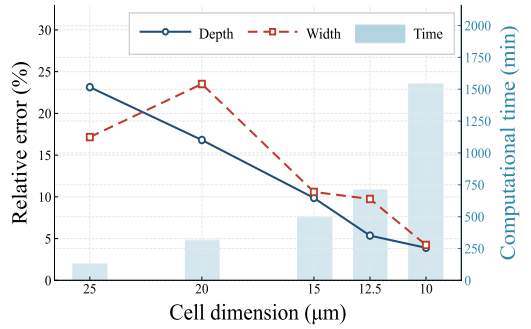

Fig. 3 High fidelity mesh study, the relative error is referred to the experimental measurements

As the mesh dimension decreases the relative error against the experimental results is reduced while, consequently by the higher number of cells, the total computational time increases. Notably, moving from 12.5 μm to 10 μm the relative error of the weld bead penetration decreases from 5.36 % to 3.90 % while the total computation time doubles. It is important to point out that the coarser mesh produced a failue in the solver.

The performance of the low-fidelity model against the mesh dimension is assessed in Fig.4 where the temperature trend of a probe located 1 mm depth inside the domain is plotted against the time for both the reference high-fidelity model (that can be considered a more reliable prediction) and three increasingly finer LF meshes. Between 2.1 and 2.7 ms the HF model does not produce any temperature data since the keyhole is present and the material is being removed. The LF model with coarse mesh has oscillating temperature spikes that can be linked to the laser moving from one element to the next. All the three meshes show a similar trend for the material heat up, capturing the transition to the liquid phase. The cooling phase after the passage of the laser source is more accurate as the mesh becomes finer, however, the LF model tends to always underestimate the temperature gradient.

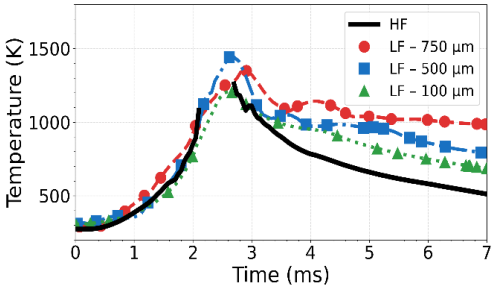

Fig. 4 Temperature trend exported from the low-fidelity model at various mesh size compared to the ground truth (high-fidelity)

Unlike numerical models, the predictive capability of PINNs is non-monotonic with respect to the network architecture. Fig. 5a shows a 2D heat map of the total loss after 50,000 optimizer iterations, plotted as a function of the number of hidden layers and neurons per layer, with all other hyperparameters held constant. Successful training runs are marked with circles, while failed runs, i.e. where the loss diverged, are marked with crosses. The results reveal a clear optimal region around 64 neurons per layer: below this value the model lacks sufficient capacity; while exceeding it leads to increased loss and training instability. This behavior is consistent with the vanishing gradient problem, which becomes more severe as network depth increases. However, architecture alone does not fully govern the model's performance. As shown

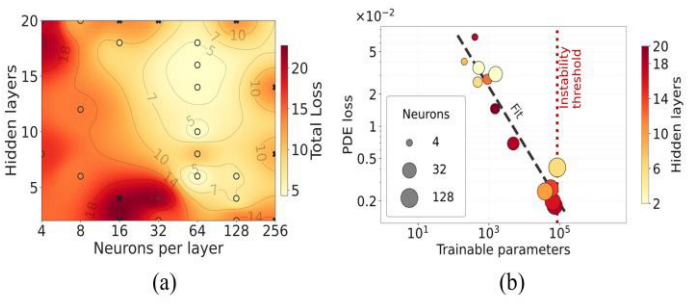

Fig. 5 Pinn losses after 50000 optimizer iterations at varying network architecture

in Fig. 5b, the PDE loss is more directly linked to the total number of trainable parameters, with instability emerging beyond approximately 10^5 parameters. At the same time, a minimum number of hidden layers is necessary to capture the high non-linearity of both the material properties and the volumetric heat source.

Fig. 6 shows a side-by-side comparison of the experimental (Fig. 6a) and predicted weld cross-sections of the validating process parameter set. All three models achieve good agreement in terms of bead depth and width, with relative errors on bead depth and width of ~4% and ~19% for the LF model, ~6–8% for the PINN, and ~5% for the HF model. However, notable differences emerge in the quality of the predicted geometry. The LF model (Fig. 6c) correctly reproduces the overall bead dimensions but, by construction, cannot capture any surface deformation or fluid-driven features, yielding a smooth and symmetric profile. The PINN (Fig. 6d), sharing the same governing equations as the LF model but differing in how the PDE residual is approximated and calibrated independently, inherits the same limitations while showing a slightly different bead shape. This is expected and reflects both the independent calibration procedures and the well-known tendency of PINNs to produce smoother solutions in regions of sharp gradients, as the network naturally regularizes the solution across the domain. In contrast, the HF model (Fig. 6b), by explicitly resolving the fluid dynamics and free surface evolution through the VOF method, which ensures mass conservation by construction, is capable of partially reproducing the periodic humping observed on the top surface of the experimental cross-section, a well-known hydrodynamic instability driven by Marangoni flow and recoil pressure within the keyhole. This qualitative agreement demonstrates that the higher physical realism in the HF model translates into geometrical detail that lower-fidelity approaches fundamentally cannot provide.

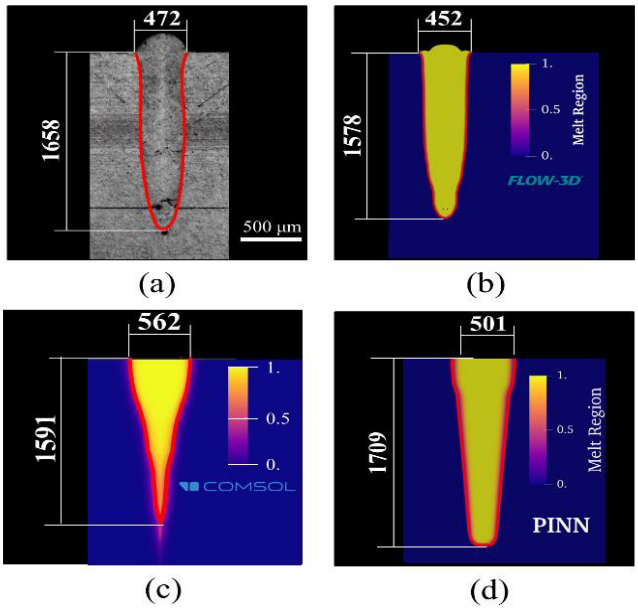

Fig. 6 Comparison between experimental (a), HF (b), LF (c), and PINN (d) weld bead cross sections

Regarding computational cost, the LF model requires approximately 10 minutes per simulation run, the HF model approximately 12.5 hours for the validation case, while the PINN incurs a one-time training cost of approximately 50 hours but delivers near-instantaneous predictions thereafter (<1 ms). It must be noted that calibration time is not included for the LF and HF models, as it depends on the number of iterations required to match the experimental data and is not directly quantifiable, unlike the PINN where training and calibration are performed in a single measurable step.

3. Conclusions

A comparison between three modelling frameworks for laser beam welding was presented. The influence of modelling strategy on predictive accuracy and computational cost was systematically assessed.

The HF model demonstrated superior physical realism, capturing temperature field dynamics during both heating and cooling stages, as well as surface deformation features such as humping, details inaccessible to lower-fidelity approaches.

However, this comes at a significantly higher computational cost. Both the LF model and the PINN achieved acceptable accuracy in predicting weld bead dimensions, representing viable alternatives when computational efficiency is prioritized. For the PINN, a non-monotonic relationship between network architecture and training performance was identified. While the PDE residual loss decreases with the total number of trainable parameters, a critical threshold exists, in the order of 10^5 parameters for the present model. This finding highlights that PINN performance cannot be improved indefinitely by increasing model complexity.

References

[1] Katayama S. Handbook of laser welding technologies. Cambridge: Woodhead publ; 2013.
[2] Sproesser G, Chang Y-J, Pittner A, et al. Life Cycle Assessment of welding technologies for thick metal plate welds. J Clean Prod 2015;108:46–53.
[3] Dal M, Fabbro R. [INVITED] An overview of the state of art in laser welding simulation. Opt Laser Technol 2016;78:2–14.
[4] Cline HE, Anthony TR. Heat treating and melting material with a scanning laser or electron beam. J Appl Phys 1977;48:3895–900.
[5] Goldak J, Chakravarti A, Bibby M. A new finite element model for welding heat sources. Metall Trans B 1984;15:299–305.
[6] Piandoro S, Fortunato A, Liverani E, et al. Numerical investigation of pulsed welding on aluminum alloy with a dual-region laser source: Exploring non-equal pulse parameters, 2025, p. 2130–40.
[7] Farrag A, Yang Y, Cao N, et al. Physics-Informed Machine Learning for metal additive manufacturing. Prog Addit Manuf 2025;10:171–85.
[8] Piandoro S, Zha D, Liverani E, et al. A Physics-Informed Neural Network–Based Framework For Near-Real-Time Keyhole Laser Welding Simulation. J Manuf Sci Eng 2026;148:071001.
[9] Linstrom P. NIST Chemistry WebBook, NIST Standard Reference Database 69 1997.
[10] Farrokhi F, Endelt B, Kristiansen M. A numerical model for full and partial penetration hybrid laser welding of thick-section steels. Opt Laser Technol 2019;111:671–86.